Chapter III

Hand-Held Paper Micro-Device with Integrated 3D Cascade for the Detection of Albumin in Serum Sample

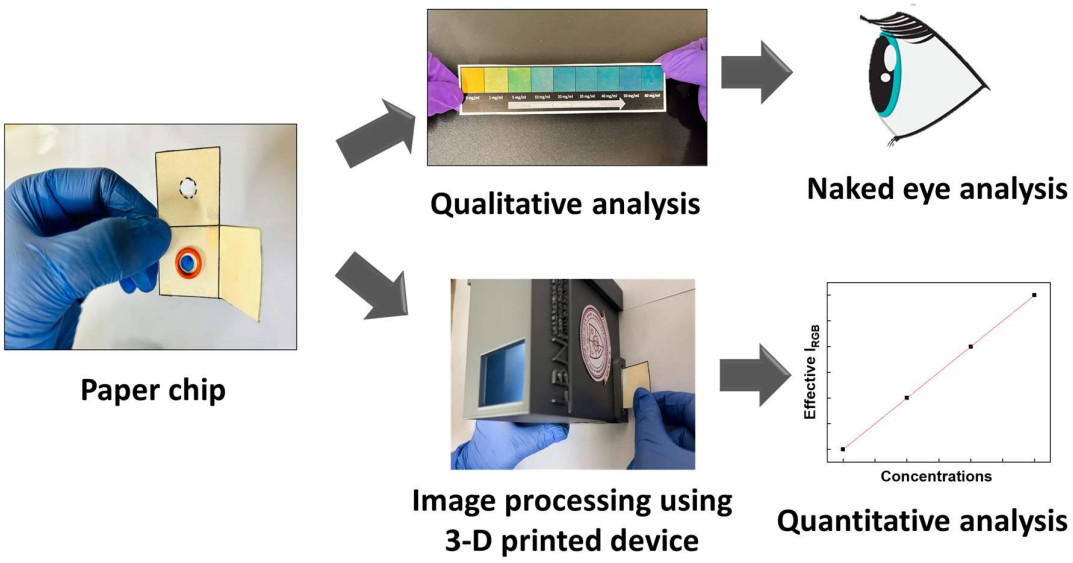

Divya et. al, *Int. Jon. of Biological Macromolecule, 2023, Vol 258, 942-949*

1. Introduction

Paper-based optical sensors have been increasingly popular in recent years because of their advantages in terms of cost, speed, and portability for environmental, health diagnostics in areas with limited resources [1,2]. Due to their speed, portability, ease of use, low sample volume requirements, and ability to perform rapid analyses, paper-based sensors have gained interest as testing tools for the identification of analytes. A number of portable and user-friendly point-of-care diagnostic tools for colorimetric analysis have been recently reported using smartphone-based lab-on-a-chip devices [3]. The cost of diagnostic testing is significantly reduced when a lab-on-a-chip device is coupled with a smartphone for point-of-care testing [4]. As compare to the conventional optical assays, paper-based biosensing devices offers user-friendly analytical module and a personalized interface that don't require bulky instruments for signal generation and their analysis [5]. The lateral flow assay technique still has a number of drawbacks despite being the most popular point-of-care platform, including a lack of quantitation capabilities and a lower level of sensitivity than the laboratory-based assays. The paper-based analytical instruments can be coupled with a variety of signal generation techniques viz colorimetric and electrochemical, where the latter is the widely adopted transduction system due to numerous advantages [6-8]. In addition to these, surface plasmon phenomenon has also been widely used in sensing of numerous molecules that are coupled with various nanostructures [9]. In colorimetry, analysis is carried out by applying reagent(s) and the target analyte to the reaction zones within the paper device. A camera and scanner are used to measure or identify changes in the assay zone color on the paper device [10-11]. The optical parameters that are utilized for image analysis while using a smartphone camera are RGB (red, green, and blue) color intensities. Rapid optical detection of body fluid biomarkers and other samples can be achieved using a smartphone with an integrated a high-resolution camera [12]. A light source for imaging, such as a light-emitting diode, light diffuser,

and optical chamber are required which offers more accurate on-site screening. Since the consistency of the optical parameters during image analysis may have an impact on the accuracy of the optical results, a closed chamber which does not allow the impact of external light is preferred. However, the high demand for these sensors forces to concentrate on affordable, rapid, and portable platforms that may be used for on-site monitoring. To fabricate them, Whatman grade 1 chromatographic paper and Whatman no. 1 filter paper have been extensively used [13-14], which contain more than 98% cellulose. Clean surface, consistent thickness, high hygroscopic qualities, wicking capabilities, flow rate, and cost effectiveness are all features of paper. Another reason for the presence of filter paper all around is that the primary component of paper i.e., cellulose fibre, is compatible with biological systems/receptors, therefore providing edge for effective colorimetric detection. These factors make paper-based sensors potentially useful in a variety of sectors, such as environmental monitoring and medical research [15-16].

The protein that the liver secretes and is most prevalent in the bloodstream is human serum albumin (ALB). The transport of fatty acids, steroids, hormones, and some medicines are the primary roles of ALB, along with maintaining the osmotic pressure in the plasma [17]. Healthy individuals typically have ALB concentrations of 35 - 50 mg/mL in their serum [18-19]. Variation in the ALB levels drastically effects on fluid balance, molecular transport, dietary intake, inflammatory markers, and immunological response in kidney dysfunction. Detection of such proteins in biological sample necessitates the creation of rapid and specific technique for detecting extremely low amounts of these analytes with high precision.

Immunosensors have drawn the most attention in the field of biosensors because they combine the specificity of an immunoreaction with the extremely high sensitivity of the analytical devices [20]. The most common method in clinics for ALB detection is based on the change in UV-Spectrophotometer signals after reaction with various dyes. Different dye-

binding technique for ALB determination include Biuret method [21], Lowry method [22], Bradford method [23], and Bromocresol Green method. These approaches are, however, subject to a number of limitations, including multi-step procedure, high sample volume, compromised dynamic range, and bulky instrumentation that limit these assay in resource limited areas [24]. In addition to these methods for ALB measurement in serum, various biosensors of different types such as fluorescence, optical, and electrochemical have also been developed [25–27]. These developed sensors have not been employed in primary health care centre because of the requirement of sophistication and skilled personal. Hence, in this work we have tried to overcome the existing problem related to ALB detection viz. quantitative estimation in miniaturized setup, fast analysis in low sample, personalized diagnostic module etc. This has been achieved by employing Anti-ALB on a bioengineered micro-sized paper device.

In this study, we have developed a bioengineered paper micro-device for the detection of ALB in the serum sample. The device was designed using filter paper as a matrix material and after that paper surface was engineered for the immobilization of antibody using a bioconjugation reaction. **Figure 3.1** systematically shows the fabrication process of the reaction zone **(a)**, reaction principle **(b)**, device designing and overall data analytics **(c)** for qualitative and quantitative analysis of ALB. The developed sensing surface was characterized using different techniques such as optical analysis, FTIR, SPM, and XPS. Additionally, 3-D printed device was designed and fabricated for performing the optical analysis in a closed environment with a controlled and constant light source. The system can quantify the ALB concentrations in clinically relevant range and in the serum samples with a high precision. The developed method is able to detect ALB in qualitative, semi-quantitative, and quantitative way.

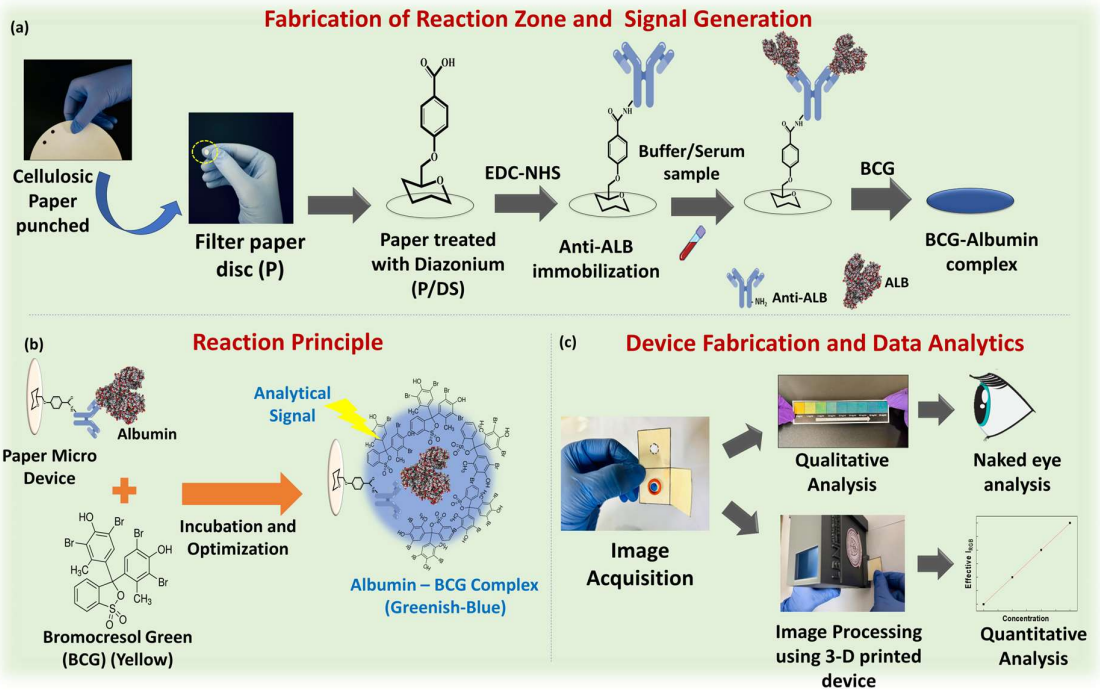

Figure 3.1: (a) *Schematic representation of step-by-step fabrication of the reaction zone and signal generation;* ***(b)*** *Reaction principle and signal generation on the surface of paper micro device;* ***(c)*** *Real image of data analytics system using a color strip and 3-D printed device for qualitative and quantitative analysis, respectively*

2. Experimental Section

2.1 Materials and Chemicals

Anti human serum albumin (Anti-ALB) antibodies were purchased from Santa Cruz Biotech., Inc. 4-aminobenzoic acid, Globulin was purchased from Sigma-Aldrich, USA. Other analytical grade chemicals such as, Tris-HCl, n-hydroxysuccinimide (NHS: $C_4H_5NO_3$), 1-(3 dimethyl aminopropyl) 3-ethyl carbodiimide hydrochloride (EDC: $C_8H_{17}N_3.HCl$), sodium nitrite ($NaNO_2$), ascorbic acid ($C_6H_8O_6$), Hydrochloric acid (HCl), bromocresolgreen (BCG), human serum albumin (ALB), disodium hydrogen phosphate (Na_2HPO_4), potassium dihydrogen phosphate (KH_2PO_4), Uric acid ($C_5H_4N_4O_3$), K^+, Alanine($C_3H_7NO_2$), Glucose ($C_6H_{12}O_6$), Glutamine ($C_5H_{10}N_2O_3$), Ascorbic Acid ($C_6H_8O_6$), Creatinine ($C_4H_7N_3O$), Homocysteine, Lipase and bovine serum albumin were purchased from SRL, India. Standard serum (RM

9955), Cysteine, and Tween-20 was procured from Hi-media, Maharashtra, India. Glutathione (BDH Biochemical), Lysozyme (Amresco, Inc), Ribonuclease (SRL India) was graciously provided by Prof. Arvind Mohan Kayastha, Department of Biotechnology, Banaras Hindu University, Varanasi. Trypsin was purchased from Edna Biolabs, India. The grade 1 Whatman filter paper was purchased from Whatman, Merck-Millipore, U.S.A. EDC/NHS was prepared in 0.1 M PBS (pH -5). PBS buffer was prepared using the standard protocol [28]. For optical measurements, 0.01 mg/mL BCG samples were prepared in 70 % ethanol which was stabilized with PBS buffer [29].

2.2 Fabrication of the Reaction Zone

Grade 1 Whatman filter sheets have been used as a substrate for the designing of reaction zone by cutting the paper in circular disc (diameter ~ 0.5 cm) form using the office punching machine. The paper disc (P) was predominantly activated with diazonium salt (DS) for 6 hours by completely immersing in DS solution in order to activate by introducing the carboxyl group onto the paper surface. The previously reported process has been followed for the preparation of the DS [16]. The activated circular discs were washed with PBS buffer to remove excessive diazonium and the activated surface was termed as P/DS. Further, the modified P/DS surface was treated with EDC/NHS (110 mM:110 mM) solution, forming a highly reactive molecule called o-acylisourea when EDC combines with the activated carboxylic group that DS introduced. NHS then reacts with this to create an ester, which then swiftly reacts with an amine (the $-NH_2$ group of the Anti-ALB antibody) to form a stable amide bond. The developed surface after reacting with EDC-NHS labelled as P/DS/EDC-NHS were washed with PBS to remove unreacted EDC-NHS on the surface. After that, Anti-ALB antibody was immobilised on the P/DS/EDC-NHS surface, which is further washed to remove unbound complex on the paper surface. For better understanding, the reaction zone after Anti-ALB immobilization was further denoted as P/DS/EDC-NHS/Anti-ALB. The FTIR, SPM, and XPS methods were used to

thoroughly characterize each modification step of the reaction zone. After validation, the strips were used to conduct the ALB detection experiment using the final P/DS/EDC-NHS/Anti-ALB sensor probe.

2.3 Instrumentation

Fourier Transform Infrared Spectroscopy (FTIR) (Nicolet iS5, THERMO Electron Scientific Instruments LLC) was used for analysis of functional groups presents on the paper surface with every successive modification and bond formation. The transmittance mode was used to acquire the spectra. X-ray photoelectron spectroscopy (XPS) (K-Alpha, Thermo Fisher Scientific) was performed for the analysis of chemical elements and functional groups before and after every modification steps. Scanning Probe Microscopy (SPM) (NTEGRA Prima, NT-MDT Service & Logistics Ltd.) was used to confirm the change occurring on the paper surface following surface engineering at every step. 3D image and micrograph assessment of the paper surface was conducted for all the modified P, P/DS, P/DS/EDC-NHS, and P/DS/EDC-NHS/Anti-ALB surfaces using Nova Px Software.

2.4 Optical Measurements

The color intensity of the reaction surface was analysed by Photoshop™ software. A particular area was fixed and selected in a circular form, and the image pixels are distributed by graphing the pixel number for each color intensity level. The RGB histogram was analysed for the selected area of the paper surface which shows intensity of every individual color and provide other statistical details that helps in determining the color intensity change. This change in color intensity is directly proportional to the ALB concentrations which eventually leads to quantification of ALB. This views information about a range of values of a highlighted region considering the collective intensity of color or a single-color channel (i.e., red in this case).

3. Results and Discussion

3.1 Reaction Zone Characterization

On each stage of the reaction probe fabrication, the paper-based reaction zone was first confirmed using FTIR. The spectra obtained after FTIR across multiple paper substrates are shown in **Figure 3.2(a)**. The stretching vibration of O-H and C-H for the P surface were found to be at 3340 cm^{-1} and 2910 cm^{-1}, respectively. Between 1000 and 1250 cm^{-1} characteristic peaks were also noted suggesting the C-C-C vibrations of the P surface **(Figure 3.2a(i))**. The carboxyl (C=O) group present in the P/DS was identified by a prominent peak at 1640 cm^{-1} following the DS treatment **(Figure 3.2a(ii))**. The addition of the carboxyl groups to the paper substrate caused these illustrative peaks to appear. After applying EDC-NHS to the P/DS surface, two distinct peaks were seen at 1639 cm^{-1} and 1476 cm^{-1} as a result of the amide I and amide II groups, respectively **(Figure 3.2a(iii))**. These amide bonds bending vibrations were created on the P/DS/EDC-NHS surface by the interaction of NHS with the carboxybenzyl flanking groups that were inserted by previous treatment. The sharp distinctive peak observed at 1640 cm^{-1} after Anti-ALB immobilisation was caused by the C=O stretching vibrations of amide I. The peak at 1544 cm^{-1} was due to the N-H bending and C-N stretching vibrations of amide II found in the peptide moiety of Anti-ALB **(Figure 3.2a(iv)**. These amide I and amide II bonds confirm the successful immobilisation of the Anti-ALB antibody on the P/DS/EDC-NHS surface.

In addition to FTIR, XPS was also performed for further confirmation of elements and functional group present on the surfaces after each step of modifications. **Figure 3.2(b)** represents the XPS survey spectra for the elements present in all the surfaces starting with bare filter paper to every modified surface. The S2p, C1s, N1s, and O1s peaks are represented in XPS spectra which are majorly due to the direct ejection of electrons. Not all peaks observed in XPS data may be attributed to the direct ejection of an electron through contact with photon.

The most prominent are the Auger peaks for example OKLL at ~ 1000 eV BE and CKLL ~ 1200 eV BE have been represented in **Figure 3.2(b)**. The peaks of OKLL shows the energy of the electrons that are released from the atoms as a result of a L shell electron occupying the O 1s state (K shell) and a L shell electron being ejected from the atom [30]. Similarly, the peaks of CKLL represents the energy of the electrons which are ejected from the atoms because a L shell electron occupying the C 1s state (K shell) and an ejection of L shell atom. The kinetic energies of the Auger peak electrons are solely determined by the electronic state of the element responsible for the emitted electron. In contrast to the photoelectric lines, modifying the X-ray characteristic energy does not result in a displacement of the Auger lines in the acquired spectra relative to a kinetic energy scale [31]. Hence the OKLL and CKLL peaks in all the different surfaces are observed at the same values of binding energy i.e., ~ 1000 eV and ~ 1200 eV, respectively. The percentage of all the elements in every surface has been represented in **Table 3.1.**

Table 3.1: *Representation of the % of elements presents in every modified surface obtained from XPS*

Modified Surface	Atomic % (C)	Atomic % (O)	Atomic % (N)	Atomic % (S)
P	41.4	58.6	0	0
P/DS	60.88	38.36	0.76	0
P/DS/EDC-NHS	59.46	39.48	0.97	0.1
P/DS/EDC-NHS/Anti-ALB	66.99	20.22	11.86	0.92

Figure 3.2(b) indicate the comparison of individual elements present on every surface for instance **Figure 3.2(c-f)** represents the S2p, C1s, N1s, and O1s spectra, respectively. **Figure 3.2(c)** shows the S2p spectra where no peaks were observed for P and P/DS surface, however a sharp peak at 167.9 eV appeared due to the SO_x bonds present in the chemical structure. After immobilization of anti-ALB peaks at 161.1 eV, 163.4 eV, 164.7 eV, 167.3 eV appeared due to

presence of disulfide and other bonds indicating the anchoring of antibody. The deconvoluted S2p peaks after anti-ALB immobilization represents various bonds such as S-H, S-C $2p_{3/2}$, S-C $2p_{1/2}$, S-S bonds and up and down spins $2p_{3/2}$, $2p_{1/2}$ of S-C. Such representative bonds and spins have also been reported for the antibody immobilization [32], suggesting the successful anchoring of anti-ALB in our case.

Further, C1s spectra (**Figure 3.2(d)**) was analysed where sharp peak at 286.4 eV was observed due to C-O-C bond which is an integral chemical functionality of cellulose (P). At P/DS surface, a representative peak at 284.5 eV appeared due to C-OH, which attributes to the presence of acidic group in DS, indicating its successful grafting. After this, the P/DS/EDC-NHS surface was analysed, where in addition to the peaks at 284.5 eV and 286.4 eV, a faint peak also appeared at 287.7 eV due to C=O. This was due to the ester bond formed after the EDC-NHS reaction on the modified P/DS surface. After immobilisation of Anti-ALB (P/DS/EDC-NHS/Anti-ALB), a highly distinct peak at 284.5 eV appeared due to the C-OH. Not only this, a signature peak at 287.7 eV was also appeared due to C=O. These are the representative peaks majorly present in the peptide backbone. Further, N1s spectra (**Figure 3.2(d)**) was examined where no peaks were observed for P surface. While analysing P/DS and P/DS/EDC-NHS surface, faint peak at 399.48 eV was observed, that was due to the nitrogenous groups present in their chemical structure. It was interesting to note that an extremely sharp and distinct peak was observed at 399.48 eV appeared due to the C-N bonds. This was due to the successful conjugation between the $-NH_2$ group of Anti-ALB and -COOH group of P/DS/EDC-NHS modified surface. Further, O1s spectra (**Figure 3.2(e)**) was analysed, a significant peak at 532.38 eV were observed due to the O-H bond present in P, P/DS, and P/DS/EDC-NHS structure. Interestingly, a predominant peak was observed at 531.21 eV representing the presence of C=O bonds in the Anti-ALB structure which was present in peptide bond of the antibody structure. These results clearly indicate the successful

development of paper micro-device which involves surface chemistry and controlled immobilization of Anti-ALB.

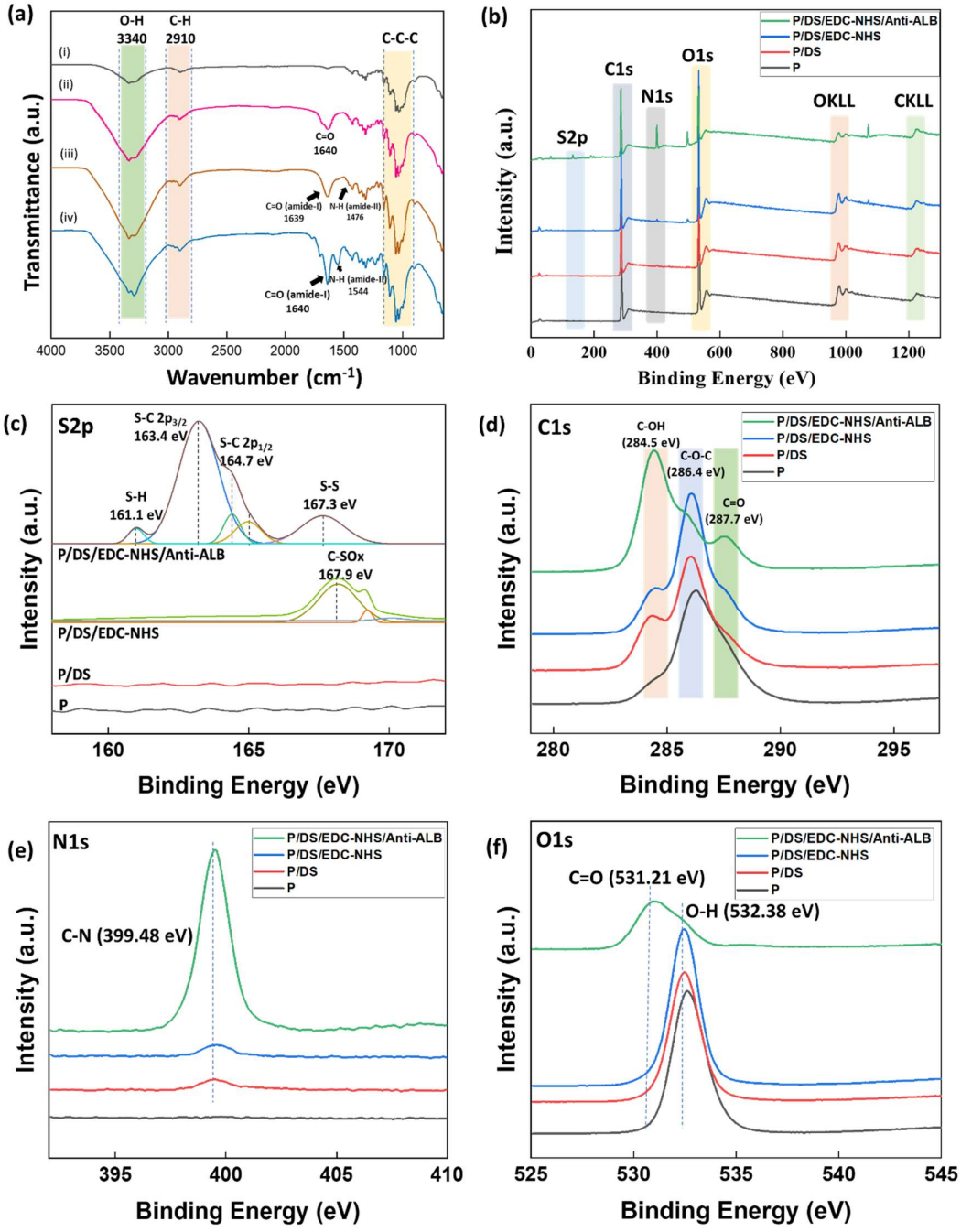

Figure 3.2: ***(a)*** *FTIR Spectra after every modification performed on the paper surface* ***(i)*** *P,* ***(ii)*** *P/DS,* ***(iii)*** *P/DS/EDC-NHS,* ***(iv)*** *P/DS/EDC-NHS/Anti-ALB;* ***(b)*** *XPS survey spectra of all the modified surfaces showing the different elements present* ***(c)*** *S2p peaks,* ***(d)*** *C1s peaks,* ***(e)*** *N1s peaks,* ***(f)*** *O1s peaks*

After confirming the functional groups and the elements present on the surface of paper and each of the modified surface. The surface topography of each layer has been analysed by performing the SPM imaging of all the surfaces in tapping mode. Following each modification, the surface topographies were captured for every synthesized reaction zone using SPM (represented in **Figure 3.3**). The z-deflection was assessed by using NOVA Px for every surface. The untreated P surface shows an evenly distributed patterns and a z-deflection value of 121 nm **(Figure 3.3(a))**. After the treatment of DS, the surface topology changed and wider structural patterns were observed. Not only this, a significant increment in z-deflection value was observed and is found to be 223 nm **(Figure 3.3(b))**. These critical observations are due to the DS activation at the P surface. After treating the surface with EDC-NHS, relatively larger crusts were observed with substantial higher z-deflection of 321 nm **(Figure 3.3(c))**. In the final step after Anti-ALB immobilisation the surface topology changed and the z-deflection value further increased to 427 nm **(Figure 3.3(d))**.

The findings of FTIR, XPS and SPM clearly suggest that the surface chemistry has been correctly performed and the antibodies are anchored in a covalent manner owing to its stability. In biological interactions, it is extremely critical to evaluate the functional antibodies i.e., their interaction with the corresponding antigen. Hence, further investigations were performed using the immunoreactions at the P/DS/EDC-NHS/Anti-ALB modified surface, where the ALB were allowed to react.

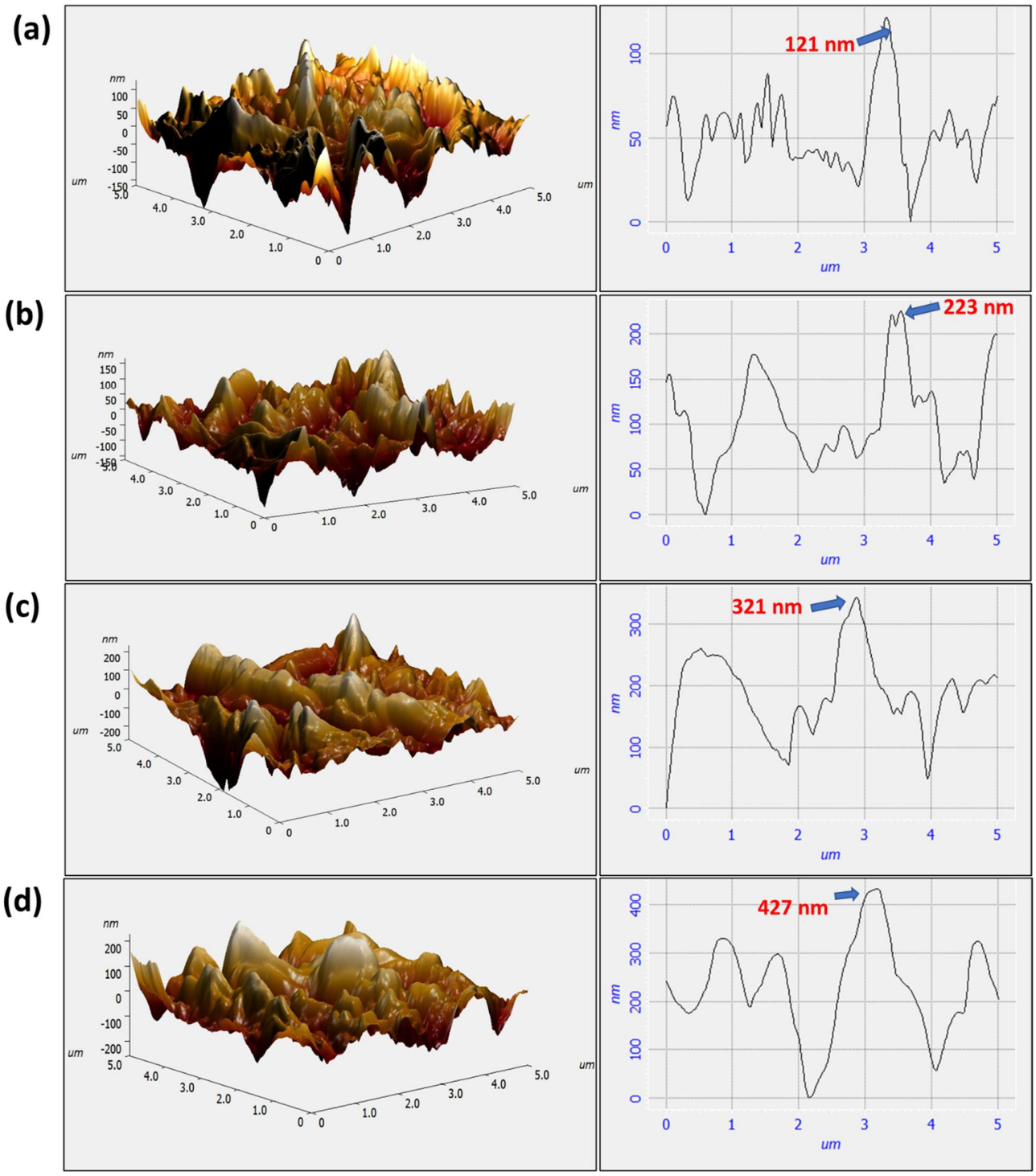

***Figure 3.3**: SPM Images showing 3-D surface and z-deflection of **(a)** P (z = 121 nm), **(b)** P/DS (z = 223 nm), **(c)** P/DS/EDC-NHS (z = 321nm), **(d)** P/DS/EDC-NHS/Anti-ALB (z = 427nm)*

3.2 Selection of color channel and confirmation of immunoreaction

The P/DS/EDC-NHS/Anti-ALB surface was allowed to react with target analyte ALB, which was further allowed to react with BCG, generating the blueish-green color. It is worth mentioning that the concentration of the BCG was kept constant to avoid any variations in the optical readouts. The generation of the signals is a function of molecular interactions between the Anti-ALB and ALB. Further, the color generation was analysed to determine and choose the optical channel which is the major cause of change in color. Thus, to obtain the maximum sensitivity, the device first analyzes the three primary colors (RGB). The three different color intensities have been compared with respect to time in order to choose which color channel is responsible for change in maximum intensity. The varying time interval was set to acquire the image of the final sensing probe P/DS/EDC-NHS/Anti-ALB/ALB/BCG with ALB concentration of 50 mg/mL. The effective intensity for each RGB intensity of the color generated and individual intensity have been calculated using the **equation 1**, reported previously [33,34]:

$$\boldsymbol{Effective\ I_{RGB}} = \mathbf{log_{10}} \frac{\boldsymbol{I_{RGB}(Blank)}}{\boldsymbol{I_{RGB}(ALB)}} \qquad \textbf{equation 1}$$

where, I_{RGB} (Blank) represents the mean pixel intensity of the final sensing probe after addition of sample, P/DS/EDC-NHS/Anti-ALB/ALB and I_{RGB} (ALB) represents the mean pixel intensity of the final reaction zone after addition of dye, P/DS/EDC-NHS/Anti-ALB/ALB/BCG surface.

The plot in **Figure 3.4(a)** shows I_{RGB} values of all three different colors (RGB) that have been obtained after BCG interaction with the P/DS/EDC-NHS/Anti-ALB/ALB surface from 0 to 40 sec. The color /signal generation starts after 10 sec and reaches at the saturation point around 40 sec. The data obtained after signal generation on the reaction zone P/DS/EDC-NHS/Anti-ALB/ALB/BCG greatly depends on the change in red channel intensity. Further, the time-dependent analysis suggests that after 30 sec, there is no significant change in the intensity was observed, indicating the reaction completion. The obtained pattern of the individual intensities

is plotted in **Figure 3.4(b)** and the corresponding regression equation for Red (I_{Red}), Green (I_{Green}), and Blue (I_{Blue}) are as follows:

$$\textit{Effective } I_{Red} = 0.0073\ (\pm\ 0.0010)\ x\ \textit{Time} + 0.0373\ (\pm\ 0.0216)$$

$$\textit{Effective } I_{Green} = 0.0003\ (\pm\ 0.0002)\ x\ \textit{Time} + 0.0228\ (\pm\ 0.0039)$$

$$\textit{Effective } I_{Blue} = 0.0015\ (\pm\ 0.0005)\ x\ \textit{Time} + 0.0389\ (\pm\ 0.0114)$$

It was observed that the I_{Red} curve has the highest slope, which was ~ 26 times and ~ 5 times larger compared to the I_{Green} and I_{Blue}, respectively. It is also noted that after the 40 sec, the maximum intensities were found to be 0.2487 (± 0.0062) a.u. for I_{Red}, 0.0295(±0.0052) a.u. for I_{Green} and 0.0910(±0.0046) a.u for I_{Blue}.

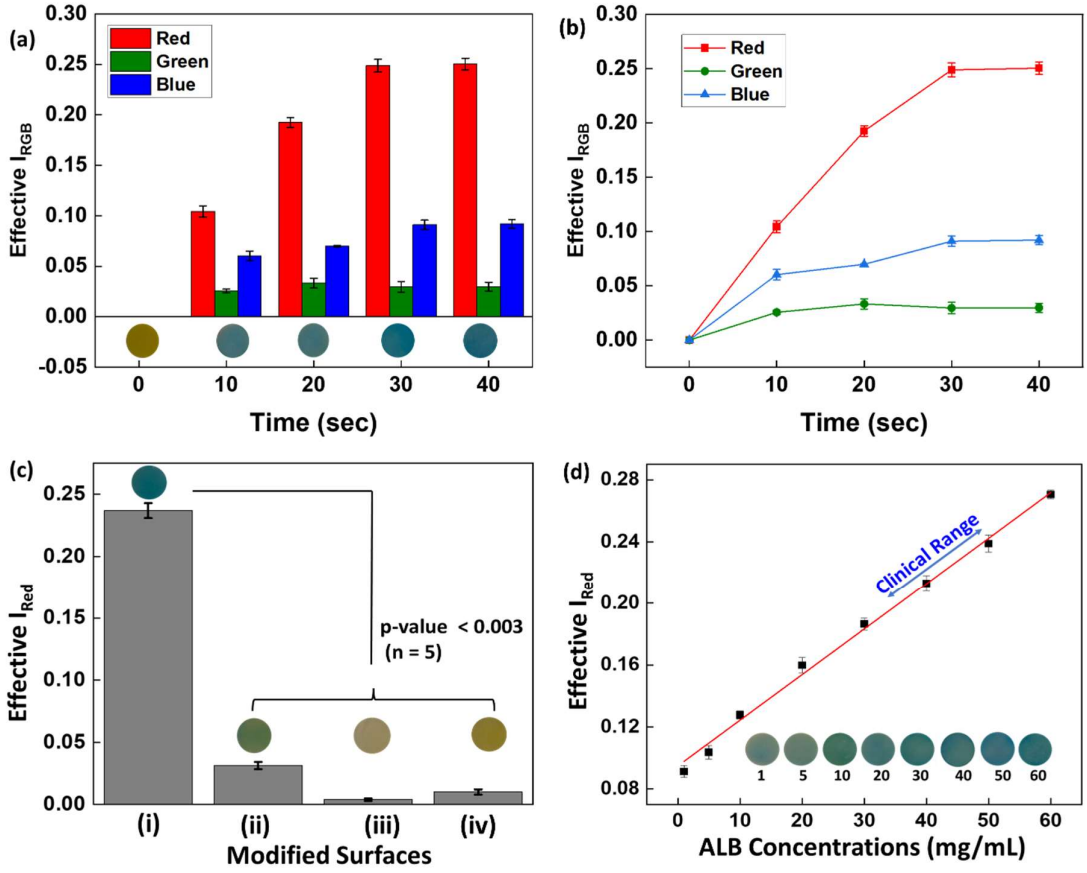

Figure 3.4: (a) *Histogram showing the change in color intensity of RGB along with the real image of disc showing time-dependent color change,* ***(b)*** *Regression curve for all the three color intensities,* ***(c)*** *Effective* I_{Red} *of different control reactions:* ***(i)*** *P/DS/EDC-NHS/Anti-ALB/ALB/BCG,* ***(ii)*** *P/DS/ALB/BCG,* ***(iii)*** *P/DS/EDC-NHS/Anti-ALB/ALB,* ***(iv)*** *P/DS/EDC-NHS/Anti-ALB/BCG,* ***(d)*** *Standard calibration graph showing linear dynamic ranges of albumin from 1 to 60 mg/mL.*

Therefore, we have selected the I_{Red} intensity for determining the ALB concentrations and 40 sec of signal generation time. Thus, the signal generated in final reaction zone after the reaction of BCG with P/DS/EDC-NHS/Anti-ALB/ALB reaction zone will be measured by focussing on the I_{Red} intensity for further experimentation.

3.3 Control Studies and System Validation

After successful fabrication of the reaction zone and determining the color channel for the final reaction, we confirmed that the color generation is solely due to the immunocomplexation followed by interaction of BCG. To validate this, a series of controlled experiments were performed. Such controlled experiments are extremely important to verify that the signal generated are not false-positive, and hence helps in proving the functionality and reliability of the ALB sensing device. In all the controlled experiments it is important to mention the concentration of Anti-ALB, ALB, and BCG were kept constant to avoid any undesirable fluctuations in the analytical signals. First, the ALB reacted with the final P/DS/EDC-NHS/Anti-ALB sensing probe to form P/DS/EDC-NHS/Anti-ALB/ALB, which was further treated with BCG, generating blueish-green color (**Figure 3.4c(i)**). After that, under the similar experimental conditions the first control reaction was performed in which ALB was allowed to react with only the diazonium-activated reaction area (P/DS), where Anti-ALB was not immobilised (**Figure 3.4c(ii)**). In this case a minor I_{Red} intensity was found, 0.031 (± 0.002) which is ~ 7.5 times less compare to the final probe (**Figure 3.4c(i)**). The statistically insignificant signal in this control experiment is most likely due to the faint reaction between the adsorbed ALB and BCG. In the next control experiment, the ALB immunocomplexed surface P/DS/EDC-NHS/Anti-ALB/ALB was directly examined, where BCG was not allowed to react. In this negative control experiment as expected, no color is generated on the reaction area proving the importance of BCG in generating the measurable analytical signals (**Figure 3.4c(iii)).** In addition to these, we also performed another control experiment where ALB was

not allowed to react with the probe followed by BCG reaction. It was interesting to note that, in this case no signals were observed (**Figure 3.4c(iv))**, proving that the immunocomplexed surface with BCG is must to generate the signals to estimate the analytical performance of the paper micro-device. These control studies shows that the analytical signals are merely due to the P/DS/EDC-NHS/Anti-ALB/ALB/BCG and no false positive signals are generated. These results were statistically evaluated by a t-test and the obtained p-value was <0.003; n = 5.

3.4 Analytical Performance

After proving the final reaction, the analytical performance of the developed sensor was examined for ALB detection in a concentration-dependent manner. For this, the fabricated sensing zone was utilized and the engineered surface P/DS/EDC-NHS/Anti-ALB was treated with varying concentrations of ALB between 1 and 60 mg/mL, which also covers the clinical ranges. The observed I_{Red} intensity values were plotted to obtain the dose dependent behaviour of the fabricated final sensing probe (**Figure 3.4(d))**. Based on the obtained results, a calibration plot was obtained and the regression equation is expressed as follows:

$$\textbf{Effective } I_{Red} \textbf{ (a.u.) = 0.0029(±0.000074) [ALB](mg/mL) + 0.0949(±0.00257),}$$

with R^2 value of 0.98. The detection limit of the developed device for ALB was determined using **equation 2** which was obtained to be 0.049(±0.002) mg/mL.

$$\textit{LOD = 3.3(SD/S)} \qquad \textit{equation 2}$$

where, SD represents the standard deviation of the blank measurements, and S represents the slope of the calibration curve.

All the experimental data and the calculations are based on the mean values obtained from 5 times repetition of the experiment. The LOQ was also calculated using the **equation 3** and the obtained value was 0.152 (±0.005) mg/mL.

$$\textit{LOQ = 10(SD/S)} \qquad \textit{equation 3}$$

where, SD represents the standard deviation of the blank measurements, and S represents the slope of the calibration curve.

The obtained detection limit is significantly lower and robust compare to the reported ALB sensors with an optical readout system. **Table 3.2** provides a detailed description of the analytical performance of various optical sensors developed for ALB detection in terms of sensor design, dynamic range, detection limit, reaction time, instrumentation required, clinical range, miniaturization ability, and as well as real sample.

Table 3.2: *Comparison of globally developed optical ALB sensors in terms of designing, analytical performance, and clinical parameters (NR= Not Reported)*

S. No.	Description	Dynamic Range	Detection Limit	Signal Generation Time	Instrumentation Required	Clinical Range	Miniaturized setup	Sample Volume	Real Sample	Ref.
1	A dual-state emissive fluorophore was integrated with paper-based sensor	10 - 50 g/L	0.91 mg/mL	< 3 min	No	Yes	Yes	5 µL	Serum matrix	[35]
2	A fluorescent probe having aggregation-induced emission property used for sensitive and specific detection	0 - 200 mg/L	0.253 mg/L	60 min	Yes	Yes	No	2 mL	Urine matrix	[36]
3	2',7'-dichlorofluorescein used as a fluorescent probe for quantification of HSA	NR	NR	> 15 min	Yes	NR	No	2 mL	Serum matrix	[37]
4	A dual-modal supramolecular based sensor using H and J-aggregated of a cyanine dye used for specific detection	0 - 400 mg/L	NR	40 min	Yes	Yes	No	NR	Urine matrix	[38]
5	a paper-based chip was developed for HSA detection utilizing heat induced reaction	0 - 5 g/dL	NR	12 min	No	Yes	Yes	10 µL	Serum matrix	[39]
6	Paper-based chip was integrated with microfluidics system	3.68 - 81.0 mg/mL	3.68 mg/mL	6 min	No	Yes	Yes	10 µL	Serum matrix	[40]
7	Twisted intramolecular charge transfer based fluorescent probe for imaging HSA	0.001 - 0.1 mg/mL	0.0013 mg/mL	5 min	Yes	No	No	2 µL	Plasma matrix	[41]
8	**Anti-ALB immobilized paper micro device for specific quantification using 3-D printed device**	**1 - 60 mg/mL**	**0.049 mg/mL**	**10 sec (saturation time 40 sec)**	**No**	**Yes**	**Yes**	**5 µL**	**Serum matrix**	**This work**

3.5 Interference Study

The selectivity must be assessed because it is one of the most important factors in order to determine clinical usefulness of the device. Therefore, under the similar experimental conditions, the selectivity assay was carried out using the molecules that are primarily present in the serum matrix, namely uric acid, K^+, alanine, glucose, glutamine, ascorbic acid, creatinine, glutathione, homocysteine, cysteine, and some proteins such as globulin, lysozyme, trypsin, lipase, and ribonuclease. **Figure 3.5(a)** demonstrates a comparative histogram of the interfering molecules and ALB, where no significant signals were observed for the interferents. This is due to the anchored antibody that specifically detects ALB. In order to simulate our results to more realistic model, we mixed all the interfering molecules with the ALB and examined. Interestingly, the signals obtained in this case was 98.32 % similar, indicating that our analytical system is very powerful and is able to detect the ALB even in heterogenous mixture. The selectivity of the device was calculated mathematically by figuring out the selectivity coefficient (K_{Sel}) using **equation 4**:

$$K_{Sel} = \frac{(Signal)_{interferent}}{(Signal)_{ALB}} \qquad \textbf{equation 4}$$

where K_{Sel} represents the selectivity coefficient, $(Signal)_{interferent}$ is the analytical signal obtained for the interfering molecules, and $(Signal)_{ALB}$ is the analytical signal obtained for the ALB molecule.

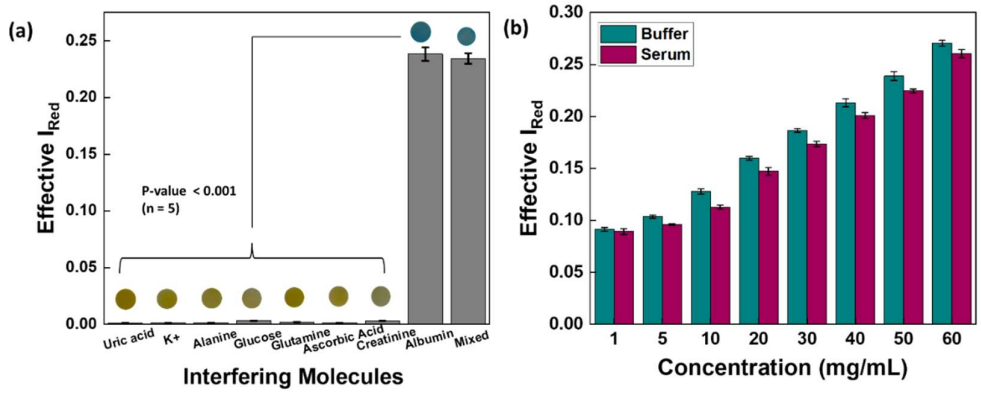

Figure 3.5: (a) *Selectivity assay of final paper micro-device for the tested interfering molecules and mixed-sample analysis,* ***(b)*** *Histogram representing the concentration-dependent ALB concentrations employing the immunosensing device in standard buffer and serum samples*

K_{sel} of the interfering molecules was found to be less than 1, which shows that the proposed sensor is very sensitive and selective for ALB. The obtained I_{Red} intensity of all the interfering molecules along with their k_{sel} was represented in **Table 3.3**. Additionally, the p-value for the interfering molecules found in the serum sample against ALB was calculated using the t-test. The readings are statistically insignificant, as evidenced by the observed p-value of <0.001 (n = 5).

Table 3.3: *Description of the obtained Effective I_{Red} intensity, K_{sel} and RSD (relative standard deviation) of the interfering molecules*

S. No.	Interfering Molecules	Effective I_{Red}	% RSD	K_{sel}
1	Uric Acid	0.0011 (±0.00005)	4.67	0.004
2	K+	0.0012 (±0.00002)	2.36	0.005
3	Alanine	0.0013 (±0.00004)	3.20	0.005
4	Glucose	0.0031 (±0.00010)	3.35	0.013
5	Glutamine	0.0020 (±0.00010)	5.21	0.008
6	Ascorbic Acid	0.0011 (±0.00006)	5.39	0.004
7	Creatinine	0.0031 (±0.00006)	1.97	0.013
8	Globulin	0.0021 (±0.00012)	4.76	0.008
9	Lysozyme	0.0027 (±0.00008)	2.96	0.011
10	Lipase	0.0023 (±0.00010)	4.34	0.009
11	Ribonuclease	0.0036 (±0.00013)	3.57	0.015
12	Glutathione	0.0026 (±0.00012)	4.61	0.010
13	Trypsin	0.0024 (±0.00009)	3.92	0.010
14	Homocysteine	0.0022 (±0.00010)	4.59	0.009
15	Cysteine	0.0019 (±0.00006)	3.42	0.008
16	Albumin	0.2383 (±0.00595)	2.49	1

3.6 Analysis in Serum Sample

ALB, a protein that is normally found in serum and is used as a marker for different health conditions [24]. Hence, its quantification in various physiological samples becomes one of the important aspects of diagnosis. Therefore, we detected ALB in serum sample to evaluate the performance capability of the developed device. First, the serum samples were processed using standard operating procedures as handled in clinics [42]. Thereafter, in order to minimise the matrix effect, it was equilibrated with PBS and then different concentrations of the ALB was injected into it. The I_{Red} intensity increases linearly with the increase in the ALB levels in the serum samples. A standard calibration plot was obtained with the regression equation as follows: Effective I_{Red} = 0.0032(±0.000168) [ALB](mg/mL) + 0.0918(±0.002) and a R^2 of 0.98. A comparative analytical performance of the sensing probe in standard buffer and serum samples have been illustrated in **Figure 3.5(b)**. The recovery percent of ALB from the serum samples at various concentrations was calculated using **equation 5**:

$$\%\ \boldsymbol{Recovery} = \frac{[\boldsymbol{P}]_{\boldsymbol{ALB}} - [\boldsymbol{Q}]_{\boldsymbol{ALB}}}{[\boldsymbol{R}]_{\boldsymbol{ALB}}}\ \boldsymbol{x}\ \mathbf{100} \qquad \textbf{equation 5}$$

where $[P]_{ALB}$ and $[Q]_{ALB}$ is the ALB concentrations for the spiked and blank sample respectively; $[R]_{ALB}$ is the amount that was observed using the standard buffer solution.

The % recovery study shows that the sensor can detect the ALB between 88.14 % and 97.70 % from the tested serum samples. The analytical performance including recovered amount of ALB, RSD, and percent recovery for all the different concentrations is shown in **Table 3.4**.

Table 3.4*: Description of the recovered ALB concentrations, % recovery, and RSD using the developed sensor in serum matrix*

S. No.	Spiked Concentrations (mg/mL)	Recovered Concentrations (mg/mL)	% Recovery	RSD (%)
1	1	0.97 (±0.01)	97.70	1.29
2	5	4.63 (±0.20)	92.74	4.48
3	10	8.81 (±0.46)	88.14	5.22
4	20	18.41 (±0.80)	92.07	4.36
5	30	27.92 (±1.40)	93.08	5.02
6	40	36.13 (±0.65)	90.34	1.80
7	50	47.03 (±2.20)	94.08	4.68
8	60	57.74 (±1.62)	96.23	2.81

3.7. Stability and Reproducibility Test

The final reaction zone (P/DS/EDC-NHS/Anti-ALB), which was tested weekly for ALB detection and reported as I_{Red}, was kept at 4 °C in a moist condition. Additionally, a study was conducted to determine the shelf-life of the developed probe. In this investigation, the probe I_{Red} was evaluated for every seven days. The sensor system maintains its activity of 94.61 %, according to the I_{Red} values, up to the three weeks. After four weeks, the signal decreased up to 86.4%, which was most likely due to the denaturation of Anti-ALB and/or degradation of the chemical modification steps. The four weeks acceptable shelf life of the sensing device probe is most likely due to the steady immobilisation of the Anti-ALB and the retention of its biological activity during storage. The device was also examined for intraday and interday variations, and it was found that the signal was consistent with minor variation of < 4.8 %, indicating that the analytical module is highly reproducible and effective. Additionally, the repeatability of the device was examined, and it was found that even when the identical

fabrication methods were used the RSD was < 3.9% and the disc-to-disc RSD was < 4.1%. These minute changes were presumably noticed may be due to the minor variation in the fabrication process of the paper micro-device and/or may be due to the handling errors.

4. Device Design and Fabrication

All of the investigations and testing results in buffer and real sample demonstrated that the developed sensing device has the potential of simply quantifying the concentration of ALB that aids in the diagnosis of CKD in clinical ranges. For the ease of its implementation in resource limited settings and at the primary healthcare centres, we developed a simplified testing setup that comprises two components of testing modules. The device has been designed in two parts including the ALB paper micro device **(Figure 3.6)** and a cascaded 3-D printed imaging device **(Figure 3.7)**. The paper micro device has been developed by designing three different pads including sensing pad, sample, and lid by printing on a filter paper using HP Ink Tank Wireless 419 printer. All the three different pads were developed in a squarical dimension of 3.0 cm x 3.0 cm and different modification was done on the sample and sensing pad as shown in **Figure 3.6(i)**. Sample pad was coated with wax manually after cutting the sample area in a circular form with a diameter of 0.5 cm so that the sample properly reaches to the reaction zone without interacting / staying on sample pad. The sensing pad was designed by coating of transparent film on the filter paper followed by placing an O-ring with an external diameter of 1 cm (internal diameter of 8 mm). After that, the developed reaction zone disc (diameter of 0.5 cm) was placed in O-ring area for precise sensing of ALB concentrations. Additionally, the final probe (P/DSEDC-NHS/anti-ALB) was set up to quantify the concentrations of ALB onto the paper micro device with the designed reaction area. The O-ring onto the surface of sensing pad provides a fixed spot for the reaction zone that allows to perform the reaction in a concise area that simplifies the process of measuring the color intensity. A transparent sheet was used on the sensing pad plays a major role in improving the need of sample volume and specificity. This

allows the sample to react only at the reaction zone, but not to other undesirable regions, contributing toward better sensitivity and selectivity. After that ALB paper device was used for experimentation and the change in color before and after the reaction with BCG was shown in **Figure 3.6(b)**. A color-based test strip has also been developed that allows the user to qualitatively monitor the ALB concentrations in a broader range in the sample matrix (**Figure 3.6(c)).** Also, the final foldable device which can be stored and carried easily, and weight of the paper micro-device was shown in **Figure 3.6(d) and 3.6(e),** respectively.

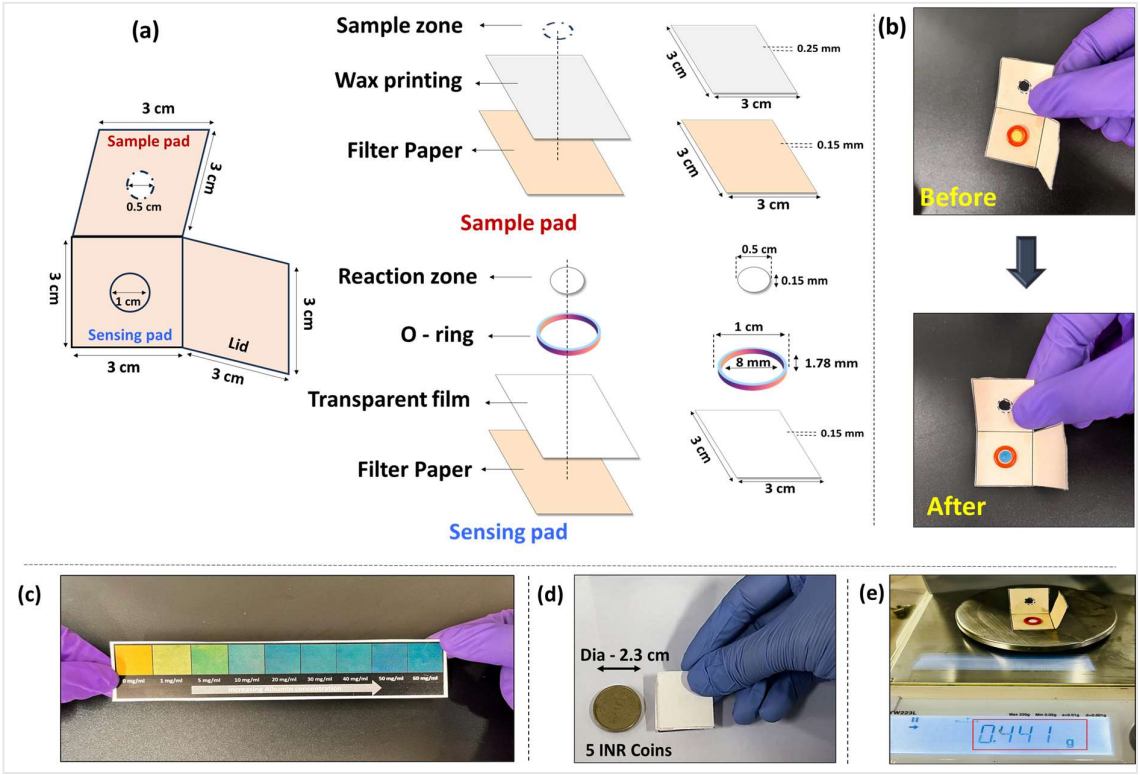

Figure 3.6: (a) *Design and dimensions of all the three different pads of the developed paper micro device,* ***(b)*** *real images before and after ALB detection,* ***(c)*** *test strip developed for qualitative/semi-quantitative determination of ALB,* ***(d)*** *paper microdevice showing the size comparison with a five-rupee Indian coin,* ***(e)*** *weight of the paper device*

The imaging device has been designed using a 3-D printer (PRUSA MINI) utilizing PLA (poly lactic acid) filament with the device dimensions of 8.5 cm (L) × 7 cm (W) × 11 cm (H). The design of the device was developed using CAD (computer-aided design) model in stl format which was further sliced for printing using Prusa G-code software. Step-by-step

fabrication of the device starting with designing of CAD model for the device, 3-D printing and designing device with in-build light source was represented in **Figure 3.7**. A passage was designed in which a fixed LED light source attached with an inbuilt battery (3200 mAh, 3.7 V) was used for providing proper and equal distribution of light during measurement of color intensity. The constant and fixed supply of light source plays an important role in providing more effective and consistent results as surrounding light usually affect the color intensity. A smartphone camera (iphone 13, 12 MP + 12 MP dual camera) was used for image capturing and the processing was done using Photoshop software. This set up lessen the requirement for a carefully regulated laboratory environment that eventually speed up the diagnosis process. The dimension of the camera passage (4.5 cm x 2.5 cm) and the strip holder (3.1 cm × 0.5 cm) which was designed for proper insertion of the sensing pad. Since the color rendering index values have a significant impact on image processing when utilizing a smartphone camera, uniform lighting must be provided. The imaging box unifies the ambient lighting conditions to offer a test platform that can be easily replicated.

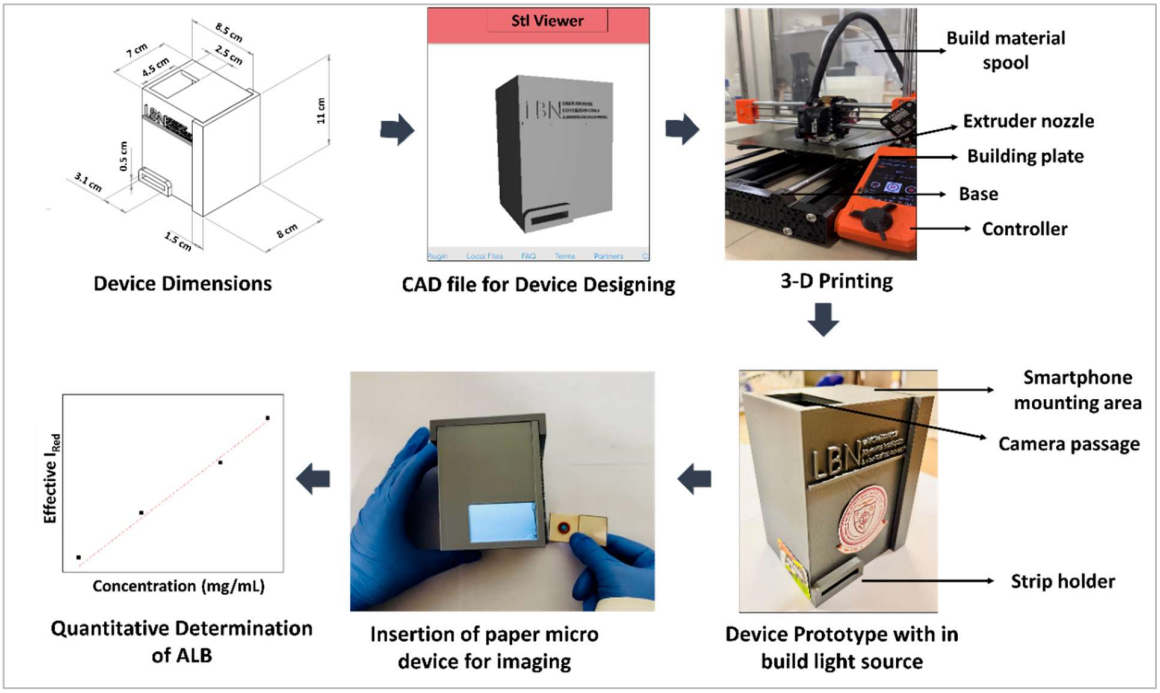

Figure 3.7: *Step-by-step process of designing of 3-D printed device with embedded light source for albumin quantification*

5. Conclusion

We have developed a paper micro-device that uses an antibody-immobilized surface to quantify ALB in a simplified manner for resource constraint areas. The bioengineered paper reaction zone was characterized using FTIR, SPM, XPS, and optical parameters. With strong consistency and linearity, the optical methodology employing parameters shows the best promise for the ALB quantification. The developed device showed linear calibration in the range of 1 – 60 mg/mL for ALB concentrations with a detection limit of 0.049(±0.002) mg/mL and signal generation time of 10 sec which saturates around 40 sec. In multianalyte environment, the biosensor also showed low rates of cross-reactivity with a k_{sel} value of less than 1. The developed device can also determine the ALB concentration in serum samples effectively, with a recovery percentage of 88.14 - 97.70%. It is recommended to use the bioengineered paper within 30 days for more precise and accurate results as its activity decreases to 86.4 % after four weeks. The final hand-held device was designed with an in-built

constant light source, requires a smaller volume of sample, easy assembly process, and lower production costs than the conventional approach. We anticipate that the designed paper sensor integrated with 3-D printed device has a great deal of potential for accurate and accessible ALB detection. This platform has a great deal of potential to aid in the identification of kidney disease, boosting the likelihood of early detection because it will make routine testing more accessible across the primary healthcare centres. This could eventually lead to improved medicines and a longer life expectancy for kidney patients.

References

[1] K. Mahato, A. Srivastava, P. Chandra, Paper based diagnostics for personalized health care: Emerging technologies and commercial aspects, Biosens. Bioelectron. 96 (2017) 246–259.

[2] E. Noviana, T. Ozer, C.S. Carrell, J.S. Link, C. McMahon, I. Jang, C.S. Henry, Microfluidic Paper-Based Analytical Devices: From Design to Applications, Chem. Rev. 121 (2021) 11835–11885.

[3] A. Roda, E. Michelini, M. Zangheri, M. Di Fusco, D. Calabria, P. Simoni, Smartphone-based biosensors: A critical review and perspectives, TrAC Trends Anal. Chem. 79 (2016) 317–325.

[4] X. Huang, D. Xu, J. Chen, J. Liu, Y. Li, J. Song, X. Ma, J. Guo, Smartphone-based analytical biosensors, Analyst. 143 (2018) 5339–5351.

[5] Y. Xu, M. Liu, N. Kong, J. Liu, Lab-on-paper micro- and nano-analytical devices: Fabrication, modification, detection and emerging applications, Microchim. Acta 2016 1835. 183 (2016) 1521–1542.

[6] P. Batista Deroco, J. de F. Giarola, D. Wachholz Júnior, G. Arantes Lorga, L. Tatsuo Kubota, Paper-based electrochemical sensing devices, Compr. Anal. Chem. 89 (2020) 91–137.

[7] F. Ghasemi, N. Fahimi-Kashani, A. Bigdeli, A.H. Alshatteri, S. Abbasi-Moayed, S.H. Al-Jaf, M.Y. Merry, K.M. Omer, M.R. Hormozi-Nezhad, Paper-based optical nanosensors – A review, Anal. Chim. Acta. 1238 (2023) 340640.

[8] K. Mahato, B. Purohit, A. Kumar, P. Chandra, Paper-based biosensors for clinical and biomedical applications: Emerging engineering concepts and challenges, Compr. Anal. Chem. 89 (2020) 163–188.

[9] D. Shajari, A. Bahari, P. Gill, M. Mohseni, Synthesis and tuning of gold nanorods with

surface plasmon resonance, Opt. Mater. (Amst). 64 (2017) 376–383.

[10] B. Purohit, A. Kumar, K. Mahato, P. Chandra, Smartphone-assisted personalized diagnostic devices and wearable sensors, Curr. Opin. Biomed. Eng. 13 (2020) 42–50.

[11] F. Mazur, A.D. Tjandra, Y. Zhou, Y. Gao, R. Chandrawati, Paper-based sensors for bacteria detection, Nat. Rev. Bioeng. 2023 13. 1 (2023) 180–192.

[12] R.E. Madrid, F.A. Ramallo, D.E. Barraza, R.E. Chaile, Smartphone-Based Biosensor Devices for Healthcare: Technologies, Trends, and Adoption by End-Users, Bioengineering. 9 (2022).

[13] K. Mahato, B. Purohit, A. Kumar, P. Chandra, Paper-based biosensors for clinical and biomedical applications: Emerging engineering concepts and challenges, in: Compr. Anal. Chem., 2020.

[14] J. Hu, S.Q. Wang, L. Wang, F. Li, B. Pingguan-Murphy, T.J. Lu, F. Xu, Advances in paper-based point-of-care diagnostics, Biosens. Bioelectron. 54 (2014) 585–597.

[15] A. Haleem, M. Javaid, R.P. Singh, R. Suman, S. Rab, Biosensors applications in medical field: A brief review, Sensors Int. 2 (2021) 100100.

[16] Divya, S. Mahapatra, P. Chandra, Design and Engineering of a Palm-Sized Optical Immunosensing Device for the Detection of a Kidney Dysfunction Biomarker, Biosens. 2022, Vol. 12, Page 1118. 12 (2022) 1118.

[17] G. Rabbani, S.N. Ahn, Review: Roles of human serum albumin in prediction, diagnoses and treatment of COVID-19, Int. J. Biol. Macromol. 193 (2021) 948–955.

[18] V. Mishra, R.J. Heath, Structural and Biochemical Features of Human Serum Albumin Essential for Eukaryotic Cell Culture, Int. J. Mol. Sci. 22 (2021).

[19] L. Yu, Y. Zhang, H. Zhao, J. Fan, A squaraine dye for detection of HSA based on disassembling dimers to monomers, Microchem. J. 165 (2021) 106172.

[20] P. Suman, P. Chandra, Immunodiagnostic Technologies from Laboratory to Point-Of-

Care Testing, Immunodiagn. Technol. from Lab. to Point-Of-Care Test. (2020) 1–245.

[21] F. Sánchez Rojas, C. Bosch Ojeda, J.M. Cano Pavón, Spectrophotometry | biochemical applications, Encycl. Anal. Sci. (2019) 205–213.

[22] J.H. Waterborg, The Lowry Method for Protein Quantitation, (2009) 7–10.

[23] N.J. Kruger, The Bradford Method For Protein Quantitation, (2009) 17–24.

[24] J.T. Busher, Serum Albumin and Globulin, Clin. Methods Hist. Phys. Lab. Exam. (1990).

[25] D. Shajari, A. Bahari, P. Gill, Fast and simple detection of bovine serum albumin concentration by studying its interaction with gold nanorods, Colloids Surfaces A Physicochem. Eng. Asp. 543 (2018) 118–125.

[26] A. Jahanban-Esfahlan, A. Ostadrahimi, R. Jahanban-Esfahlan, L. Roufegarinejad, M. Tabibiazar, R. Amarowicz, Recent developments in the detection of bovine serum albumin, Int. J. Biol. Macromol. 138 (2019) 602–617.

[27] J.F. Xu, Y.S. Yang, A.Q. Jiang, H.L. Zhu, Detection Methods and Research Progress of Human Serum Albumin,. 52 (2020) 72–92.

[28] Phosphate-buffered saline (PBS), Cold Spring Harb. Protoc. 2006 (2006) pdb.rec8247.

[29] S.-J.; Chen, C.-C.; Tseng, K.-H.; Huang, Y.-C.; Chang, L.-M. Fu, S.-J. Chen, C.-C. Tseng, K.-H. Huang, Y.-C. Chang, L.-M. Fu, Microfluidic Sliding Paper-Based Device for Point-of-Care Determination of Albumin-to-Creatine Ratio in Human Urine, Biosens. 2022, Vol. 12, Page 496. 12 (2022) 496.

[30] F.A. Stevie, C.L. Donley, Introduction to x-ray photoelectron spectroscopy ARTICLES YOU MAY BE INTERESTED IN, J. Vac. Sci. Technol. A. 38 (2020) 63204.

[31] XPS Spectra, (2013). www.casaxps.com (accessed November 22, 2023).

[32] H. Mekaru, A. Yoshigoe, M. Nakamura, T. Doura, F. Tamanoi, Biodegradability of Disulfide-Organosilica Nanoparticles Evaluated by Soft X-ray Photoelectron

Spectroscopy: Cancer Therapy Implications, (2018).

[33] K. Mahato, P. Chandra, Paper-based miniaturized immunosensor for naked eye ALP detection based on digital image colorimetry integrated with smartphone, Biosens. Bioelectron. 128 (2019) 9–16.

[34] M. Lutfi Firdaus, W. Alwi, F. Trinoveldi, I. Rahayu, L. Rahmidar, K. Warsito, The 4 th International Conference on Sustainable Future for Human Security, SustaiN 2013 Determination of Chromium and Iron Using Digital Image-based Colorimetry, Procedia Environ. Sci. 20 (2014) 298–304.

[35] Z. Luo, T. Lv, K. Zhu, Y. Li, L. Wang, J.J. Gooding, G. Liu, B. Liu, Paper-Based Ratiometric Fluorescence Analytical Devices towards Point-of-Care Testing of Human Serum Albumin, Angew. Chemie - Int. Ed. 59 (2020) 3131–3136.

[36] Q. Hu, B. Yao, T.C. Owyong, S. Prashanth, C. Wang, X. Zhang, W.W.H. Wong, Y. Tang, Y. Hong, Detection of Urinary Albumin Using a “Turn-on” Fluorescent Probe with Aggregation-Induced Emission Characteristics, Chem. - An Asian J. 16 (2021) 1245–1252.

[37] S.E. Smith, J.M. Williams, S. Ando, K. Koide, Time-Insensitive Fluorescent Sensor for Human Serum Albumin and Its Unusual Red Shift, (2014).

[38] H. Sun, J. Xiang, X. Zhang, H. Chen, Q. Yang, Q. Li, A. Guan, Q. Shang, Y. Tang, G. Xu, A colorimetric and fluorometric dual-modal supramolecular chemosensor and its application for HSA detection, Analyst. 139 (2013) 581–584.

[39] R.-J. Yang, C.-C. Tseng, W.-J. Ju, H.-L. Wang, M. Fu, A rapid paper-based detection system for determination of human serum albumin concentration, (2018).

[40] R.J. Yang, C.C. Tseng, W.J. Ju, L.M. Fu, M.P. Syu, Integrated microfluidic paper-based system for determination of whole blood albumin, Sensors Actuators B Chem. 273 (2018) 1091–1097.

[41] Y. Fan, F. Wang, F. Hou, L. Wei, G. Zhu, D. Zhao, Q. Hu, T. Lei, L. Yang, P. Wang, G. Ge, A novel TICT-based near-infrared fluorescent probe for light-up sensing and imaging of human serum albumin in real samples, Chinese Chem. Lett. 34 (2023) 107557.

[42] M.K. Tuck, D.W. Chan, D. Chia, A.K. Godwin, W.E. Grizzle, K.E. Krueger, W. Rom, M. Sanda, L. Sorbara, S. Stass, W. Wang, D.E. Brenner, Standard operating procedures for serum and plasma collection: Early detection research network consensus statement standard operating procedure integration working group, J. Proteome Res. 8 (2009) 113–117.